

Fundamental properties of snake robot locomotion

Pål Liljebäck, Kristin Y. Pettersen, Øyvind Stavdahl, and Jan Tommy Gravdahl

Abstract—This paper presents a set of fundamental properties of the velocity of a snake robot conducting lateral undulation on a planar surface. In particular, the derived properties state that the average forward velocity of the snake robot 1) is proportional to the squared amplitude of the sinusoidal motion of each joint of the robot, 2) is proportional to the angular frequency of the sinusoidal motion of each joint, 3) is proportional to a particular function of the constant phase shift between the joints, and 4) is maximized by the phase shift between the joints that also maximizes the particular phase shift function. The paper presents simulation results that support the validity of the derived properties.

I. INTRODUCTION

Inspired by biological snakes, snake robots carry the potential of meeting the growing need for robotic mobility in challenging environments. Snake robots consist of serially connected modules capable of bending in one or more planes. The many degrees of freedom of snake robots make them difficult to control, but provide traversability in irregular environments that surpasses the mobility of the more conventional wheeled, tracked and legged forms of robotic mobility. Research on snake robots has been conducted for several decades. However, our understanding of snake locomotion so far is for the most part based on empirical studies of biological snakes and simulation-based synthesis of relationships between parameters of the snake robot.

There are several reported works aimed at analysing and understanding snake locomotion. Gray [1] conducted empirical and analytical studies of snake locomotion already in the 1940s. Hirose [2] studied biological snakes and developed mathematical relationships characterizing their motion, such as the *serpenoid curve*. Saito *et al.* [3] optimized the parameters of the serpenoid curve based on simulations of a planar snake robot. Hicks [4] investigated general requirements for the propulsion of a three-linked snake robot. Nilsson [5] employed energy arguments to analyse planar snake locomotion with isotropic friction. Transeth *et al.* [6] proved that the velocity of a planar snake robot is bounded. Li *et al.* [7] studied the controllability of the joint motion of a snake robot. The authors have previously studied the stability properties of snake locomotion based on *Poincaré maps* [8] and investigated the controllability properties of a planar snake robot influenced by anisotropic friction [9].

Research on robotic fish and eel-like mechanisms is relevant to research on snake robots since these mechanisms

are very similar. The works in [10]–[12] investigate the controllability of various fish-like mechanisms, synthesize gaits for translational and rotational motion based on Lie bracket calculations, and propose controllers for tracking straight and curved trajectories.

The contribution of this paper is a set of fundamental properties of the velocity dynamics of a planar snake robot that are useful from a motion planning perspective. The properties are derived based on a simplified model of a snake robot proposed by the authors in [13]. The derived properties state that the average forward velocity of a planar snake robot 1) is proportional to the squared amplitude of the sinusoidal motion of each joint of the robot, 2) is proportional to the angular frequency of the sinusoidal motion of each joint, 3) is proportional to a particular function of the constant phase shift between the joints, and 4) is maximized by the phase shift between the joints that also maximizes the particular phase shift function. To the authors' best knowledge, these fundamental properties of snake locomotion have never before been derived analytically. The paper presents simulation results that support the theoretical findings.

The paper is organized as follows. Section II presents a complex model of a snake robot that will be used for simulation purposes. Section III presents a simplified model of a snake robot that the theoretical findings are based upon. Section IV presents a controller for the snake robot. Section V derives the fundamental properties of the velocity dynamics of the snake robot. Section VI presents simulation results. Finally, Section VII presents concluding remarks.

II. A COMPLEX MODEL OF A PLANAR SNAKE ROBOT

This section summarizes a complex model of a planar snake robot previously presented in [9]. We will use this model to simulate the motion of the snake robot in Section VI.

A. Notation and defined symbols

We consider a planar snake robot consisting of N links of length l interconnected by $N-1$ active joints. The kinematics and dynamics of the snake robot are defined in terms of the symbols illustrated in Fig. 1 and Fig. 2. All N links have the same mass m and moment of inertia J . The total mass of the snake robot is therefore Nm . The mass of each link is uniformly distributed so that the link CM (center of mass) is located at its center point.

The snake robot moves in the horizontal plane and has a total of $N+2$ degrees of freedom. The position of the CM (center of mass) of the snake robot is denoted by $\mathbf{p} = (p_x, p_y) \in \mathbb{R}^2$. The absolute angle θ_i of link i is expressed with respect to the global x axis with counterclockwise positive direction. As seen in Fig. 1, the relative angle between link i and link $i+1$ is given by $\phi_i = \theta_{i+1} - \theta_i$. The local coordinate system of each link is fixed in the CM

Affiliation of Pål Liljebäck is shared between the Department of Engineering Cybernetics at the Norwegian University of Science and Technology, NO-7491 Trondheim, Norway, and SINTEF ICT, Dept. of Applied Cybernetics, N-7465 Trondheim, Norway. E-mail: Pal.Liljeback@sintef.no

K. Y. Pettersen, Øyvind Stavdahl, and Jan Tommy Gravdahl are with the Department of Engineering Cybernetics at the Norwegian University of Science and Technology, NO-7491 Trondheim, Norway. E-mail: {Kristin.Y.Pettersen, Oyvind.Stavdahl, Tommy.Gravdahl}@itk.ntnu.no

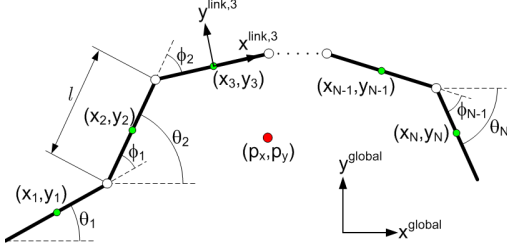


Fig. 1. Kinematic parameters of the snake robot.

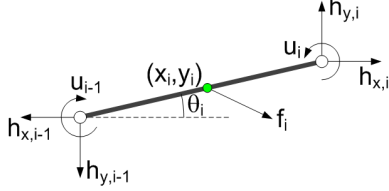


Fig. 2. Forces and torques acting on each link of the snake robot.

of the link with x (tangential) and y (normal) axis oriented such that they are oriented in the directions of the global x and y axis, respectively, when the link angle is zero. The rotation matrix from the global frame to the frame of link i is given by

$$\mathbf{R}_{\text{link},i}^{\text{global}} = \begin{bmatrix} \cos \theta_i & -\sin \theta_i \\ \sin \theta_i & \cos \theta_i \end{bmatrix} \quad (1)$$

The forces and torques acting on link i are visualized in Fig. 2. The ground friction force is denoted by f_i and acts on the CM of the link. The joint constraint forces from link $i+1$ and link $i-1$ are denoted by h_i and $-h_{i-1}$, respectively. The actuator torque applied at joint i is denoted by u_i .

B. Friction model

We will consider two ground friction models in this study, i.e. a *viscous* and a *Coulomb* friction model. Both models assume that the links have *anisotropic* ground friction properties, which is essential for efficient snake locomotion on planar surfaces.

The *viscous* ground friction is characterized by the two friction coefficients c_t and c_n describing the friction force in the tangential (along link x axis) and normal (along link y axis) direction of a link, respectively. Using (1), the viscous friction force on link i in the global frame as a function of the global link velocities, \dot{x}_i and \dot{y}_i , is defined as

$$\begin{aligned} \mathbf{f}_i &= \mathbf{R}_{\text{link},i}^{\text{global}} \mathbf{f}_i^{\text{link},i} = -\mathbf{R}_{\text{link},i}^{\text{global}} \begin{bmatrix} c_t & 0 \\ 0 & c_n \end{bmatrix} \mathbf{v}_i^{\text{link},i} \\ &= -\mathbf{R}_{\text{link},i}^{\text{global}} \begin{bmatrix} c_t & 0 \\ 0 & c_n \end{bmatrix} \left(\mathbf{R}_{\text{link},i}^{\text{global}} \right)^T \begin{bmatrix} \dot{x}_i \\ \dot{y}_i \end{bmatrix} \end{aligned} \quad (2)$$

where $\mathbf{f}_i^{\text{link},i}$ and $\mathbf{v}_i^{\text{link},i}$ are, respectively, the friction force and the link velocity expressed in the local link frame.

The *Coulomb* ground friction force is defined in a similar way by the two friction coefficients μ_t and μ_n describing the friction force in the tangential and normal direction of a link, respectively. The Coulomb friction force on link i in the global frame is defined as

$$\begin{aligned} \mathbf{f}_i &= \mathbf{R}_{\text{link},i}^{\text{global}} \mathbf{f}_i^{\text{link},i} \\ &= -mg \mathbf{R}_{\text{link},i}^{\text{global}} \begin{bmatrix} \mu_t & 0 \\ 0 & \mu_n \end{bmatrix} \text{sgn} \left(\mathbf{v}_i^{\text{link},i} \right) \\ &= -mg \mathbf{R}_{\text{link},i}^{\text{global}} \begin{bmatrix} \mu_t & 0 \\ 0 & \mu_n \end{bmatrix} \text{sgn} \left(\left(\mathbf{R}_{\text{link},i}^{\text{global}} \right)^T \begin{bmatrix} \dot{x}_i \\ \dot{y}_i \end{bmatrix} \right) \end{aligned} \quad (3)$$

where g is the gravitational acceleration constant and $\text{sgn}(\cdot)$ is the signum function.

C. Equations of motion

It is shown in [9] that the equations of motion of the snake robot in terms of the joint angles, $\phi \in \mathbb{R}^{N-1}$, the absolute angle of the head link, $\theta_N \in \mathbb{R}$, the position of the CM of the snake robot, $(p_x, p_y) \in \mathbb{R}^2$, and the joint torques, $\mathbf{u} \in \mathbb{R}^{N-1}$, can be written as

$$\begin{aligned} \ddot{\phi} &= \mathbf{u} \\ \ddot{\theta}_N &= g(\phi, \theta_N, \dot{\phi}, \dot{\theta}_N, \dot{p}_x, \dot{p}_y, \mathbf{u}) \\ Nm\ddot{p}_x &= \sum_{i=1}^N f_{x,i} \\ Nm\ddot{p}_y &= \sum_{i=1}^N f_{y,i} \end{aligned} \quad (4)$$

where $g(\phi, \theta_N, \dot{\phi}, \dot{\theta}_N, \dot{p}_x, \dot{p}_y, \mathbf{u}) \in \mathbb{R}$ is a complex function of the state vector and the joint torques. The global frame friction force on each link, represented by $f_{x,i}$ and $f_{y,i}$, is either the *viscous* friction force defined in (2) or the *Coulomb* friction force defined in (3).

III. A SIMPLIFIED MODEL OF A PLANAR SNAKE ROBOT

This section summarizes a model of a planar snake robot which is described in detail in [13]. The model forms the basis of the investigation of the fundamental locomotion properties in Section V.

A. Overview of the model

We consider a planar snake robot with links interconnected by active revolute joints. The surface beneath the robot is flat and horizontal, and each link is subjected to a viscous ground friction force. The body shape changes of the robot induce friction forces on the links that produce the translational and rotational motion of the robot. A simplified model that captures only the most essential part of the snake robot dynamics is proposed in [13]. The idea behind this model is illustrated in Fig. 3 and motivated by an analysis presented in [13], which shows that:

- The forward motion of a planar snake robot is produced by the link velocity components that are *normal* to the forward direction.
- The change in body shape during forward locomotion primarily consists of relative displacements of the CM of the links *normal* to the forward direction of motion.

Based on these two properties, the simplified model describes the body shape changes of a snake robot as *linear displacements* of the links with respect to each other instead of rotational displacements. The linear displacements occur *normal* to the forward direction of motion and produce friction forces that propel the robot forward. This essentially means that the revolute joints of the snake robot are modelled as prismatic (translational) joints and that the rotational motion of the links during body shape changes is disregarded.

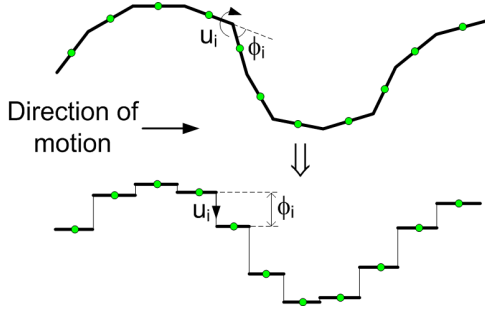


Fig. 3. The revolute joints of the snake robot are modelled as prismatic joints that displace the CM of each link transversal to the direction of motion.

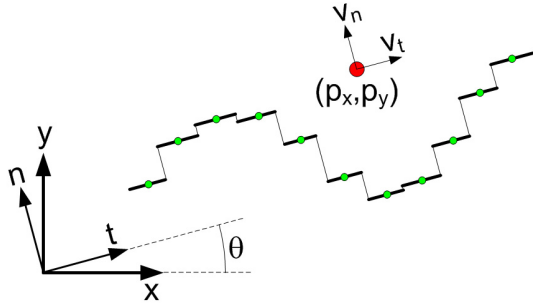


Fig. 4. Illustration of the two coordinate frames employed in the model. The global \$x-y\$ frame is fixed. The \$t-n\$ frame is always aligned with the snake robot.

However, the model still captures the *effect* of the rotational link motion during body shape changes, which is a linear displacement of the CM of the links normal to the forward direction of motion.

The model of the snake robot is summarized in the following subsections in terms of the symbols illustrated in Fig. 4 and Fig. 5.

B. Kinematics of the snake robot

The snake robot has \$N\$ links of length \$l\$ and mass \$m\$ interconnected by \$N-1\$ prismatic joints. The prismatic joints control the normal direction distance between the links. As seen in Fig. 5, the normal direction distance from link \$i\$ to link \$i+1\$ is denoted by \$\phi_i\$ and represents the coordinate of joint \$i\$. The positive direction of \$\phi_i\$ is along the \$n\$ axis.

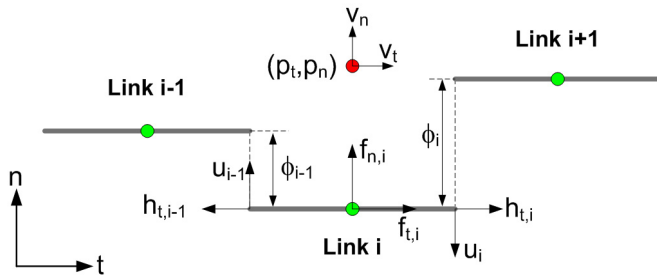


Fig. 5. Symbols characterizing the kinematics and dynamics of the snake robot.

The snake robot moves in the horizontal plane and has \$N+2\$ degrees of freedom. The motion is defined with respect to the two coordinate frames illustrated in Fig. 4. The \$x-y\$ frame is the fixed global frame. The \$t-n\$ frame is always aligned with the snake robot, i.e. the \$t\$ and \$n\$ axis always point in the *tangential* and *normal* direction of the robot, respectively. The origin of both frames are fixed and coincide.

As seen in Fig. 4 and Fig. 5, the global frame position of the CM (center of mass) of the snake robot is denoted by \$(p_x, p_y) \in \mathbb{R}^2\$, while the \$t-n\$ frame position is denoted by \$(p_t, p_n) \in \mathbb{R}^2\$. The global frame orientation is denoted by \$\theta \in \mathbb{R}\$ and is expressed with respect to the global \$x\$ axis with counterclockwise positive direction. The angle between the global \$x\$ axis and the \$t\$ axis is also \$\theta\$ since the \$t-n\$ frame is always aligned with the snake robot. The relationship between the \$t-n\$ frame and the global frame position is given by

$$p_t = p_x \cos \theta + p_y \sin \theta \quad (5a)$$

$$p_n = -p_x \sin \theta + p_y \cos \theta \quad (5b)$$

C. Equations of motion

The state vector of the model is chosen as

$$\mathbf{x} = (\phi, \theta, p_t, p_n, \mathbf{v}_\phi, v_\theta, v_t, v_n) \in \mathbb{R}^{2N+4} \quad (6)$$

where \$\phi = (\phi_1, \dots, \phi_{N-1}) \in \mathbb{R}^{N-1}\$ are the joint coordinates, \$\theta \in \mathbb{R}\$ is the absolute orientation, \$(p_t, p_n) \in \mathbb{R}^2\$ is the \$t-n\$ frame position of the CM, \$\mathbf{v}_\phi = \dot{\phi} \in \mathbb{R}^{N-1}\$ are the joint velocities, \$v_\theta = \dot{\theta} \in \mathbb{R}\$ is the angular velocity, and \$(v_t, v_n) \in \mathbb{R}^2\$ is the tangential and normal direction velocity of the snake robot.

As illustrated in Fig. 5, each link is influenced by a ground friction force (acting on the CM of the link) and constraint forces that hold the joints together. A model of these forces is presented in [13], where it is also shown that the complete model of the snake robot can be written as

$$\dot{\phi} = \mathbf{v}_\phi \quad (7a)$$

$$\dot{\theta} = v_\theta \quad (7b)$$

$$\dot{p}_t = v_t + p_n v_\theta \quad (7c)$$

$$\dot{p}_n = v_n - p_t v_\theta \quad (7d)$$

$$\dot{\mathbf{v}}_\phi = -\frac{c_1}{m} \mathbf{v}_\phi + \frac{c_2}{m} v_t \mathbf{A} \mathbf{D}^T \phi + \frac{1}{m} \mathbf{D} \mathbf{D}^T \mathbf{u} \quad (7e)$$

$$\dot{v}_\theta = -c_3 v_\theta + \frac{c_4}{N-1} v_t \bar{\mathbf{e}}^T \phi \quad (7f)$$

$$\dot{v}_t = -\frac{c_1}{m} v_t + \frac{2c_2}{Nm} v_n \bar{\mathbf{e}}^T \phi - \frac{c_2}{Nm} \phi^T \mathbf{A} \bar{\mathbf{D}} \mathbf{v}_\phi \quad (7g)$$

$$\dot{v}_n = -\frac{c_1}{m} v_n + \frac{2c_2}{Nm} v_t \bar{\mathbf{e}}^T \phi \quad (7h)$$

where \$\mathbf{u} \in \mathbb{R}^{N-1}\$ are the actuator forces at the joints and

$$\bar{\mathbf{e}} = [1 \ \dots \ 1]^T \in \mathbb{R}^{N-1},$$

$$\bar{\mathbf{D}} = \mathbf{D}^T (\mathbf{D} \mathbf{D}^T)^{-1} \in \mathbb{R}^{N \times (N-1)},$$

$$\mathbf{A} = \begin{bmatrix} 1 & 1 & & & \\ & \cdot & \cdot & & \\ & & \cdot & \cdot & \\ & & & \cdot & \cdot \\ & & & & 1 & 1 \end{bmatrix}, \mathbf{D} = \begin{bmatrix} 1 & -1 & & & \\ & \cdot & \cdot & & \\ & & \cdot & \cdot & \\ & & & \cdot & \cdot \\ & & & & 1 & -1 \end{bmatrix},$$

where $\mathbf{A} \in \mathbb{R}^{(N-1) \times N}$ and $\mathbf{D} \in \mathbb{R}^{(N-1) \times N}$. The parameters c_1 , c_2 , c_3 , and c_4 are scalar friction coefficients that characterize the external forces acting on the snake robot. More specifically, the coefficient c_1 determines the magnitude of the friction forces resisting the link motion, c_2 determines the magnitude of the induced friction forces that propel the snake robot forward, c_3 determines the friction torque opposing the rotation of the snake robot, while c_4 determines the induced torque that rotates the snake robot. This torque is induced when the forward direction velocity and the average of the joint coordinates are nonzero. The role of each coefficient is explained in more detail in [13].

IV. CONTROLLER DESIGN

The actuator forces are set according to the linearizing control law

$$\mathbf{u} = m \left(\mathbf{D}\mathbf{D}^T \right)^{-1} \left(\bar{\mathbf{u}} + \frac{c_1}{m} \dot{\phi} - \frac{c_2}{m} v_t \mathbf{A}\mathbf{D}^T \phi \right) \quad (8)$$

where $\bar{\mathbf{u}} \in \mathbb{R}^{N-1}$ is a new set of control inputs. This control law transforms the joint dynamics (7e) into $\dot{v}_\phi = \bar{\mathbf{u}}$.

We will control the snake robot according to a motion pattern called *lateral undulation* [2], which consists of horizontal waves that are propagated backwards along the snake body from head to tail. Lateral undulation is achieved by controlling joint $i \in \{1, \dots, N-1\}$ of the snake robot according to the sinusoidal reference

$$\phi_{i,\text{ref}} = \alpha \sin(\omega t + (i-1)\delta) + \phi_o \quad (9)$$

where α and ω are the amplitude and frequency, respectively, of the sinusoidal joint motion and δ determines the phase shift between the joints. The parameter ϕ_o is a joint offset coordinate used to control the direction of the locomotion. We assume that ϕ_o is a constant offset, so that

$$\dot{\phi}_{i,\text{ref}} = \alpha \omega \cos(\omega t + (i-1)\delta) \quad (10)$$

$$\ddot{\phi}_{i,\text{ref}} = -\alpha \omega^2 \sin(\omega t + (i-1)\delta) \quad (11)$$

We choose the control input $\bar{\mathbf{u}}$ of the snake robot as

$$\bar{\mathbf{u}} = \ddot{\phi}_{\text{ref}} + k_d \left(\dot{\phi}_{\text{ref}} - \dot{\phi} \right) + k_p \left(\phi_{\text{ref}} - \phi \right) \quad (12)$$

where k_p and k_d are positive scalar controller gains and $\phi_{\text{ref}} \in \mathbb{R}^{N-1}$ are the joint reference coordinates. The error dynamics of the joints is therefore given by

$$\left(\ddot{\phi}_{\text{ref}} - \ddot{\phi} \right) + k_d \left(\dot{\phi}_{\text{ref}} - \dot{\phi} \right) + k_p \left(\phi_{\text{ref}} - \phi \right) = 0 \quad (13)$$

which is clearly *exponentially stable* [14].

V. ANALYSIS OF THE VELOCITY DYNAMICS BASED ON AVERAGING THEORY

In this section, *averaging theory* [15] is employed in order to study the velocity dynamics of the snake robot during lateral undulation. We employ averaging theory since we are primarily interested in the overall, i.e. average, speed and direction of the locomotion. The periodic fluctuations about the average trajectory of the snake is not of particular interest.

A. Model of the velocity dynamics of the snake robot

The velocity dynamics of the snake robot is defined by (7f), (7g), and (7h), which give the dynamics of the forward direction velocity v_t , the normal direction velocity v_n , and the angular velocity v_θ of the snake robot. It was shown in Section IV that we can achieve exponentially stable tracking of the joint reference coordinates (9) with the control law (12). We will therefore assume that ϕ and $v_\phi = \dot{\phi}$ are given by (9) and (10), respectively. Furthermore, we assume that the amplitude α and frequency ω of the joint motion are always set according to the rule

$$\omega = \frac{k_{\alpha\omega}}{\alpha^2} \quad (14)$$

where $k_{\alpha\omega} > 0$ is a constant controller parameter. This rule allows us to write the model of the velocity dynamics in a particular standard averaging form in the next subsection. Note that α and ω are still independent parameters since any choice of α and ω can be obtained by choosing $k_{\alpha\omega} = \alpha^2 \omega$. Using (9), (10), and (14), and introducing the velocity state vector $\mathbf{v} = (v_t, v_n, v_\theta) \in \mathbb{R}^3$, the velocity dynamics can be written as

$$\dot{\mathbf{v}} = \begin{bmatrix} \dot{v}_t \\ \dot{v}_n \\ \dot{v}_\theta \end{bmatrix} = \mathbf{f}(t, \mathbf{v}) \quad (15)$$

where

$$\mathbf{f}(t, \mathbf{v}) = \begin{bmatrix} -\frac{c_1}{m} v_t + \frac{2c_2}{Nm} v_n f_1(\omega t) - \frac{c_2}{Nm} f_2(\omega t) \\ -\frac{c_1}{m} v_n + \frac{2c_2}{Nm} v_t f_1(\omega t) \\ -c_3 v_\theta + \frac{c_4}{N-1} v_t f_1(\omega t) \end{bmatrix} \quad (16)$$

$$f_1(\omega t) = (N-1) \phi_o + \sum_{i=1}^{N-1} \alpha \sin(\omega t + (i-1)\delta) \quad (17)$$

$$f_2(\omega t) = \sum_{i=1}^{N-1} \sum_{j=1}^{N-1} \left[\frac{k_{\alpha\omega}}{\alpha} \phi_o a_{ij} \cos(\omega t + (j-1)\delta) + k_{\alpha\omega} a_{ij} \sin(\omega t + (i-1)\delta) \cos(\omega t + (j-1)\delta) \right] \quad (18)$$

and where a_{ij} denotes element ij of the matrix $\mathbf{A}\bar{\mathbf{D}}$.

B. Averaged model of the velocity dynamics

The method of *averaging* [15] can be applied to systems of the form

$$\dot{\mathbf{x}} = \varepsilon \mathbf{f}(t, \mathbf{x}) \quad (19)$$

where $\varepsilon > 0$ is a small parameter and $\mathbf{f}(t, \mathbf{x})$ is T -periodic, i.e. $\mathbf{f}(t+T, \mathbf{x}) = \mathbf{f}(t, \mathbf{x})$. A system that, in ‘average’, behaves similarly to the system in (19) is given by

$$\dot{\mathbf{x}} = \varepsilon \frac{1}{T} \int_0^T \mathbf{f}(\tau, \mathbf{x}) d\tau \quad (20)$$

The smallness requirement on ε ensures that \mathbf{x} varies slowly with t relative to the periodic excitation of the system. The system response will thereby be determined predominantly by the average of the excitation.

To transform the model (15) into the standard form of averaging (19), we change the time scale from t to $\tau = \omega t$ and define $\varepsilon = 1/\omega$. Since $\frac{d}{dt} = \frac{1}{\varepsilon} \frac{d}{d\tau}$, the model (15) can now be written as

$$\frac{d\mathbf{v}}{d\tau} = \varepsilon \mathbf{f}(\tau, \mathbf{v}) \quad (21)$$

where

$$\mathbf{f}(\tau, \mathbf{v}) = \begin{bmatrix} -\frac{c_1}{m}v_t + \frac{2c_2}{Nm}v_n f_1(\tau) - \frac{c_2}{Nm}f_2(\tau) \\ -\frac{c_1}{m}v_n + \frac{2c_2}{Nm}v_t f_1(\tau) \\ -c_3 v_\theta + \frac{c_4}{N-1}v_t f_1(\tau) \end{bmatrix} \quad (22)$$

The averaged model of (21) is now given by calculating the integral in (20) and changing time scale back to t using that $\frac{d}{d\tau} = \varepsilon \frac{d}{dt}$. The resulting averaged model is shown in [16] to be given by

$$\dot{\mathbf{v}} = \mathcal{A}\mathbf{v} + \mathbf{b} \quad (23)$$

where

$$\mathcal{A} = \mathcal{A}(\phi_o) = \begin{bmatrix} -\frac{c_1}{m} & \frac{2(N-1)}{Nm}c_2\phi_o & 0 \\ \frac{2(N-1)}{Nm}c_2\phi_o & -\frac{c_1}{m} & 0 \\ c_4\phi_o & 0 & -c_3 \end{bmatrix} \quad (24)$$

$$\mathbf{b} = \mathbf{b}(\alpha, \omega, \delta) = \begin{bmatrix} \frac{c_2}{2Nm}k_{\alpha\omega}k_\delta \\ 0 \\ 0 \end{bmatrix} \quad (25)$$

and where the constant $k_\delta \in \mathbb{R}$ is defined as

$$k_\delta = \sum_{i=1}^{N-1} \sum_{j=1}^{N-1} a_{ij} \sin((j-i)\delta) \quad (26)$$

We see that the averaged model of the velocity dynamics is a linear system characterized by the parameters of the joint reference coordinates, i.e. by α , ω , δ , and ϕ_o .

C. Analysis of the velocity dynamics

The averaged model (23) has a single equilibrium point at $\mathbf{v} = -\mathcal{A}^{-1}\mathbf{b}$. By inspecting the eigenvalues of \mathcal{A} , it is shown in [16] that this equilibrium point is *globally exponentially stable* as long as the joint coordinate offset ϕ_o is below a certain threshold. This means that the average velocity of the snake robot will converge exponentially to the steady state velocity

$$\bar{\mathbf{v}} = -\mathcal{A}^{-1}\mathbf{b} = [\bar{v}_t \quad \bar{v}_n \quad \bar{v}_\theta]^T \quad (27)$$

which is given analytically by

$$\bar{v}_t = k_{\alpha\omega}k_\delta \frac{Nc_1c_2}{2(N^2c_1^2 - (4N^2 - 8N + 4)c_2^2\phi_o^2)} \quad (28a)$$

$$\bar{v}_n = k_{\alpha\omega}k_\delta \frac{\phi_o(N-1)c_2^2}{N^2c_1^2 - (4N^2 - 8N + 4)c_2^2\phi_o^2} \quad (28b)$$

$$\bar{v}_\theta = k_{\alpha\omega}k_\delta \frac{\phi_o N c_1 c_2 c_4}{2c_3(N^2c_1^2 - (4N^2 - 8N + 4)c_2^2\phi_o^2)} \quad (28c)$$

The work in [16] provides more details regarding the correspondence between the average and the exact velocity of the snake robot. The main result in [16] is basically that, for sufficiently large ω , the average velocity of the snake robot given by (23) will approximate the exact velocity given by (15) for all time, and the error of this approximation is bounded.

Eq. (27) represents an interesting result since it gives an analytical expression for the steady state velocity of a snake robot with an arbitrary number of links N as a function

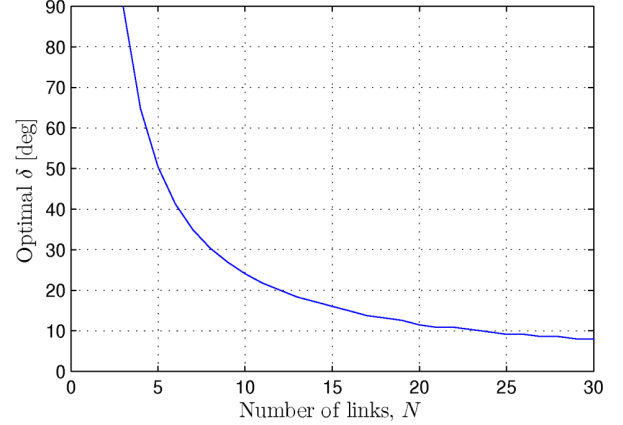


Fig. 6. The optimal phase shift δ that maximizes the forward velocity of a planar snake robot as a function of the number of links N .

of the controller parameters α , ω , δ , and ϕ_o . We can for example immediately see that the steady state velocity of the snake robot when it conducts lateral undulation with zero joint offset ($\phi_o = 0$) is given by $\bar{v}_t = \frac{c_2}{2Nc_1}k_{\alpha\omega}k_\delta$, $\bar{v}_n = 0$, and $\bar{v}_\theta = 0$. In the following, we will use this result to deduce some fundamental relationships between the forward velocity and the controller parameters of the snake robot.

The forward velocity is seen from (28a) to be proportional to the controller parameter $k_{\alpha\omega} = \alpha^2\omega$, i.e. the forward velocity is proportional to the square of the amplitude of the joint motion, α^2 , and also proportional to the angular frequency, ω , of the joint motion. This information is useful from a motion planning perspective since it tells us that an increase/decrease of the forward velocity by a certain factor can be achieved by increasing/decreasing ω by the same factor or by increasing/decreasing α by the square root of this factor.

It is also seen from (28a) that the forward velocity of the snake robot is proportional to the function k_δ defined in (26). Since k_δ is a function of the phase shift δ between the joints, this means that the phase shift δ that will maximize the forward velocity can be determined analytically as the δ that maximizes k_δ . This is particularly interesting since we are now able to analytically determine the optimal phase shift δ that maximizes the forward velocity of a planar snake robot with an arbitrary number of links N . Fig. 6 presents a plot of the maximum value of k_δ as a function of the number of links N . For each N , the maximum value of k_δ was found using the mathematical computer software *Matlab*. The optimal phase shift is e.g. $\delta = 90^\circ$ for $N = 3$ links, $\delta = 50.4^\circ$ for $N = 5$ links, $\delta = 24.1^\circ$ for $N = 10$ links, and $\delta = 11.5^\circ$ for $N = 20$ links.

The above results can be summarized as follows:

Proposition 1: Consider a planar snake robot with N links modelled by (7) and controlled in exact accordance with (9) and (10). The average forward velocity of the snake robot given by (23) will converge exponentially to a value which is proportional to:

- the squared amplitude of the sinusoidal joint motion, α^2 .
- the angular frequency of the sinusoidal joint motion, ω .
- the function of the constant phase shift, δ , between the

joints given by

$$k_\delta = \sum_{i=1}^{N-1} \sum_{j=1}^{N-1} a_{ij} \sin((j-i)\delta) \quad (29)$$

where a_{ij} denotes element i,j of the matrix $A\overline{D}$. Moreover, for a given α and ω , the phase shift, δ , that maximizes the average forward velocity is given by the δ that maximizes k_δ .

VI. SIMULATION RESULTS

Proposition 1 was derived from the simplified model of snake locomotion given by (7). The authors have verified by simulations that the velocity of the snake robot from the simplified model complies very well with the properties stated in Proposition 1. These simulation results are, however, not included in this paper due to space restrictions. Instead, the purpose of this section is to strengthen the significance of Proposition 1 by illustrating that these properties also apply to the velocity from the complex model of snake locomotion given by (4).

A. Simulation parameters

The model of the snake robot (4) was implemented and simulated in *Matlab R2008b* on a laptop running *Windows XP*. The dynamics was calculated using the *ode45* solver in Matlab with a relative and absolute error tolerance of 10^{-3} .

We considered snake robots with $N = 3$, $N = 5$, $N = 10$, and $N = 20$ links of length $l = 0.14$ m, mass $m = 1$ kg, and moment of inertia $J = 0.0016$ kgm². Both *viscous* and *Coulomb* ground friction were considered. The friction coefficients of the viscous friction model defined in (2) were set to $c_t = 0.5$ and $c_n = 3$, while the friction coefficients of the Coulomb friction model defined in (3) were set to $\mu_t = 0.1$ and $\mu_n = 0.4$.

The joints of the snake robot were controlled according to (12) with controller gains set to $k_p = 20$ and $k_d = 5$. The joint reference coordinates were calculated according to the motion pattern *lateral undulation* defined in (9) with zero joint angle offset ($\phi_o = 0$). The values of the controller parameters α , ω , and δ are presented with each simulation result. The initial state of the snake robot was $(\phi = 0, \theta_N = 0, p = 0, \dot{\phi} = 0, \dot{\theta}_N = 0, \dot{p} = 0)$.

The simulation results below present the average forward speed of the snake robot, denoted by \bar{v} , for different sets of controller parameters. This average speed was calculated at the end of each run of a simulation as the linear distance travelled by the CM of the snake robot divided by the simulation time, which was chosen to be $t_{\text{sim}} = 10$ s. The average speed was, in other words, calculated as

$$\bar{v} = \frac{\sqrt{(p_x(10) - p_x(0))^2 + (p_y(10) - p_y(0))^2}}{10} \quad (30)$$

B. Relationship between the forward velocity and α

Proposition 1 states that the average forward velocity of a planar snake robot is proportional to the squared amplitude of the sinusoidal joint motion, α^2 . We investigated the validity of this result by simulating the snake robot with different values of α and calculating the resulting average

forward velocity. The simulation results with viscous and Coulomb ground friction, respectively, are shown in Fig. 7. The number of links N and the corresponding values of ω and δ are shown at the top of each plot. The range of α values is shorter for large N compared to for small N since a large angle amplitude will cause a collision between the head and the tail of the snake when N is large. The plots clearly show an exponential increase in the forward speed \bar{v} as the amplitude α increases. This is in accordance with Proposition 1.

Note that the amplitude of the joint motion cannot be increased indefinitely. For sufficiently large α , the relative link velocity components that are *tangential* to the forward direction will no longer be negligible, which is assumed in the simplified model of the snake robot. It is reasonable to expect that the increase in the forward velocity starts to decay for large α . This decay can be seen in the plots with viscous friction in Fig. 7, which shows that the velocity increase has a more linear character when α becomes large.

C. Relationship between the forward velocity and ω

Proposition 1 states that the average forward velocity of a planar snake robot is proportional to the angular frequency, ω , of the joint motion. This result was investigated by simulating the snake robot with different values of ω and calculating the resulting average forward velocity. The simulation results with viscous and Coulomb ground friction, respectively, are shown in Fig. 8. The number of links N and the corresponding values of α and δ are shown at the top of each plot. With viscous friction, the plots show a clear linear increase in the forward speed \bar{v} as the frequency ω increases. This is in accordance with Proposition 1. With Coulomb friction, the forward speed increases linearly for $N = 3$ links. However, for $N = 5$, $N = 10$, and $N = 20$ links, the forward speed seems to increase linearly up to a certain frequency, after which the forward speed decreases. This suggests that the Coulomb friction model (3) introduces nonlinear couplings between the controller parameters α , ω , and δ that are not present when the viscous friction model (2) is used. To illustrate this nonlinear coupling further, the simulation of the snake robot with $N = 20$ links was repeated with the phase shift increased from $\delta = 11.5^\circ$ to $\delta = 20^\circ$ as shown in Fig. 9. In the Coulomb friction case, the forward speed now has a linear character over a much wider range of frequencies.

In summary, the simulation results agree very well with Proposition 1 for the case of viscous ground friction. With Coulomb ground friction, however, the linear increase of the forward speed as a function of ω is present only up to a certain frequency, which seems to depend on the other controller parameters.

D. Relationship between the forward velocity and δ

The final result stated in Proposition 1 is that the average forward velocity is maximized by the phase shift δ that maximizes the function k_δ . To investigate the validity of this result, we simulated the snake robot with different values of δ to identify the phase shift that produced the highest forward velocity. The simulation results with viscous and Coulomb ground friction, respectively, are shown in Fig. 10. The number of links N and the corresponding values of

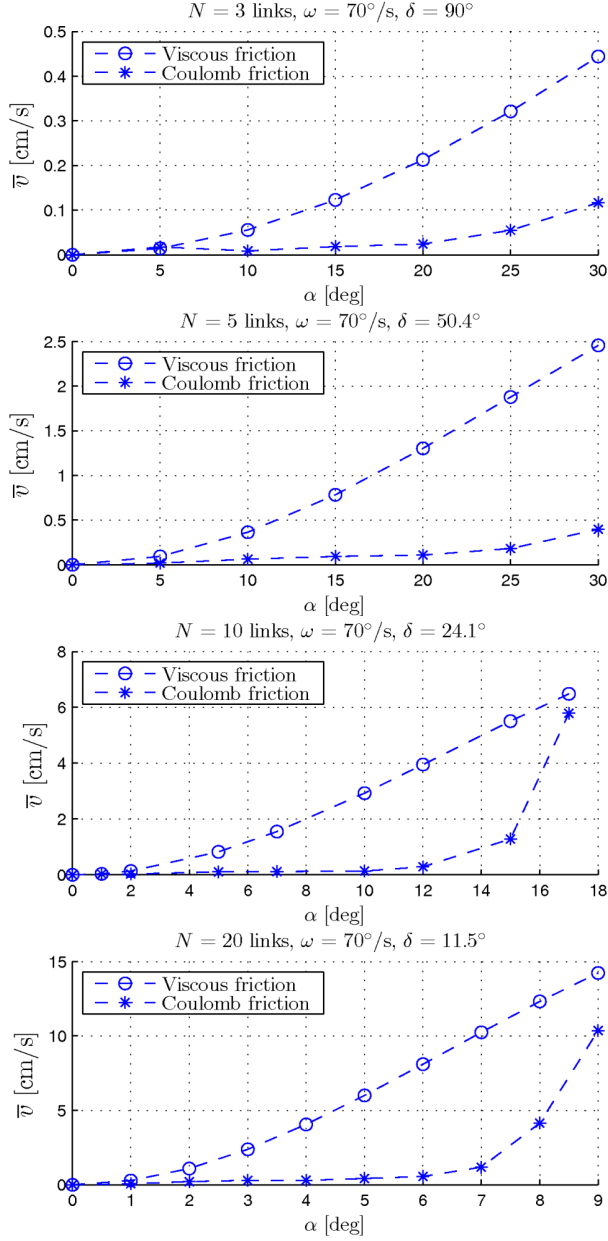


Fig. 7. The average forward velocity of the snake robot for different values of α . The number of links N and the corresponding values of ω and δ are shown at the top of each plot.

α and ω are shown at the top of each plot. The δ value that maximizes k_δ is indicated with a vertical dashed line in each plot. Except for the case of Coulomb friction with $N = 3$ links, the maximum velocity of each plot in Fig. 10 seems to agree well with the δ value that maximizes k_δ . The best agreement seems to be produced with viscous ground friction. The reason for the disagreement for the case of Coulomb friction with $N = 3$ links is probably due to nonlinear effects not captured by the simplified model of the snake robot. Note that the forward velocity in this case is very small.

In summary, the simulation results indicate that Proposi-

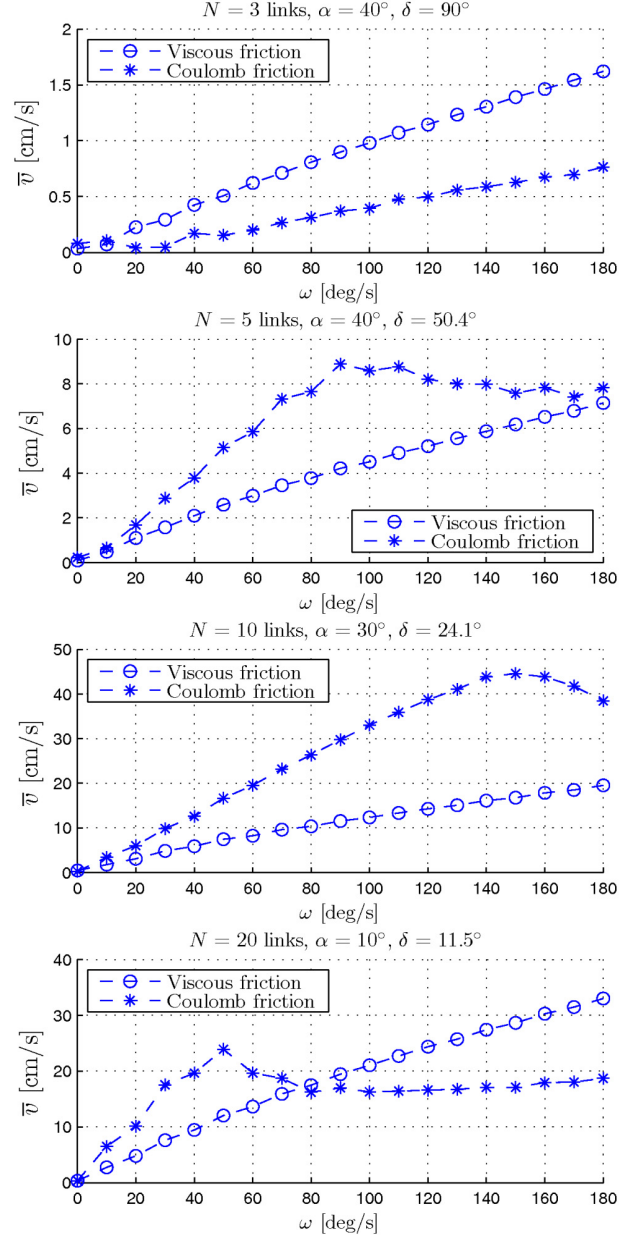


Fig. 8. The average forward velocity of the snake robot for different values of ω . The number of links N and the corresponding values of α and δ are shown at the top of each plot.

tion 1 provides a reasonable prediction of the phase shift, δ , that maximizes the average forward velocity from the complex model of snake locomotion given by (4).

VII. CONCLUSIONS AND FUTURE WORK

This paper has derived a set of fundamental properties of the velocity dynamics of a planar snake robot based on a simplified model of the robot. The properties state that the average forward velocity of a planar snake robot conducting lateral undulation is proportional to 1) the squared amplitude of the sinusoidal joint motion, 2) the angular frequency of the sinusoidal joint motion, and 3) a particular function of the constant phase shift between the joints. Moreover, the

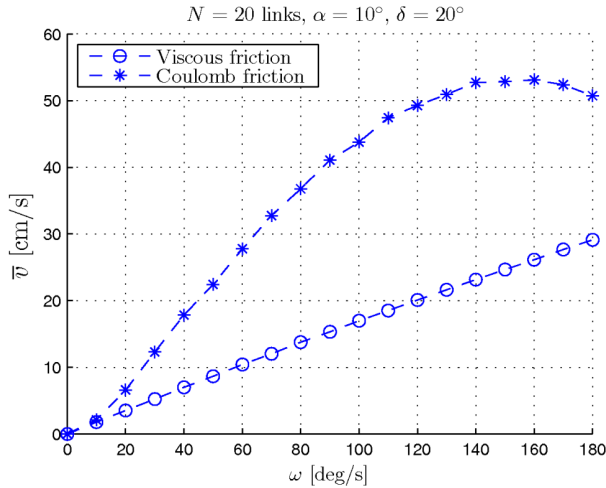


Fig. 9. A rerun of the simulation of the snake robot with $N = 20$ links from Fig. 8 with the phase shift increased from $\delta = 11.5^\circ$ to $\delta = 20^\circ$.

results showed that the phase shift between the joints that maximizes the forward velocity of the snake is given by the phase shift that maximizes the particular phase shift function. The paper has presented simulation results that support the validity of the derived properties. In future work, the authors will employ the theoretical findings in this paper in order to develop and analyse motion planning strategies for snake robots.

REFERENCES

- [1] J. Gray, "The mechanism of locomotion in snakes," *J. Exp. Biol.*, vol. 23, no. 2, pp. 101–120, 1946.
- [2] S. Hirose, *Biologically Inspired Robots: Snake-Like Locomotors and Manipulators*. Oxford: Oxford University Press, 1993.
- [3] M. Saito, M. Fukaya, and T. Iwasaki, "Serpentine locomotion with robotic snakes," *IEEE Contr. Syst. Mag.*, vol. 22, no. 1, pp. 64–81, February 2002.
- [4] G. P. Hicks, "Modeling and control of a snake-like serial-link structure," Ph.D. dissertation, North Carolina State University, 2003.
- [5] M. Nilsson, "Serpentine locomotion on surfaces with uniform friction," in *Proc. IEEE/RSJ Int. Conf. Intelligent Robots and Systems*, 2004, pp. 1751–1755.
- [6] A. A. Transeth, N. van de Wouw, A. Pavlov, J. P. Hespanha, and K. Y. Pettersen, "Tracking control for snake robot joints," in *Proc. IEEE/RSJ Int. Conf. Intelligent Robots and Systems*, San Diego, CA, USA, Oct–Nov 2007, pp. 3539–3546.
- [7] J. Li and J. Shan, "Passivity control of underactuated snake-like robots," in *Proc. 7th World Congress on Intelligent Control and Automation*, June 2008, pp. 485–490.
- [8] P. Liljebäck, K. Y. Pettersen, Ø. Stavdahl, and J. T. Gravdahl, "Stability analysis of snake robot locomotion based on poincaré maps," in *Proc. IEEE/RSJ Int. Conf. Intelligent Robots and Systems*, 2009, pp. 3623–3630.
- [9] —, "Controllability analysis of planar snake robots influenced by viscous ground friction," in *Proc. IEEE/RSJ Int. Conf. Intelligent Robots and Systems*, 2009, pp. 3615–3622.
- [10] P. A. Vela, K. A. Morgansen, and J. W. Burdick, "Underwater locomotion from oscillatory shape deformations," in *Proc. IEEE Conf. Decision and Control*, vol. 2, Dec. 2002, pp. 2074–2080 vol.2.
- [11] K. McIsaac and J. Ostrowski, "Motion planning for anguilliform locomotion," *IEEE Trans. Robot. Autom.*, vol. 19, no. 4, pp. 637–625, August 2003.
- [12] K. Morgansen, B. Triplett, and D. Klein, "Geometric methods for modeling and control of free-swimming fin-actuated underwater vehicles," *IEEE Transactions on Robotics*, vol. 23, no. 6, pp. 1184–1199, Dec 2007.

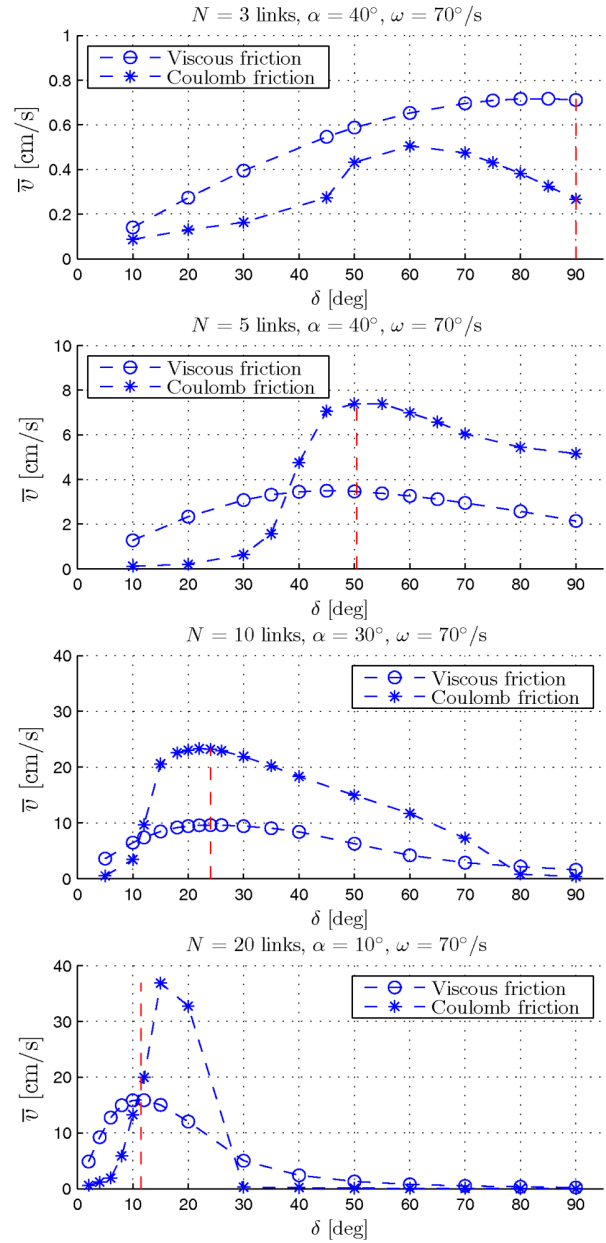


Fig. 10. The average forward velocity of the snake robot for different values of δ . The number of links N and the corresponding values of α and ω are shown at the top of each plot.

- [13] P. Liljebäck, K. Y. Pettersen, Ø. Stavdahl, and J. T. Gravdahl, "A simplified model of planar snake robot locomotion," in *Proc. IEEE/RSJ Int. Conf. Intelligent Robots and Systems*, 2010, accepted.
- [14] H. K. Khalil, *Nonlinear Systems*, 3rd ed. Prentice Hall, 2002.
- [15] J. A. Sanders, F. Verhulst, and J. Murdock, *Averaging Methods in Nonlinear Dynamical Systems*, 2nd ed., ser. Applied Mathematical Sciences. Springer, 2007, vol. 59.
- [16] P. Liljebäck, K. Y. Pettersen, Ø. Stavdahl, and J. T. Gravdahl, "Stability analysis of snake robot locomotion based on averaging theory," in *Proc. IEEE Int. Conf. Decision and Control*, 2010, submitted.